Journal of Fluids and Structures 130 (2024) 104176

Contents lists available at ScienceDirect

Journal of Fluids and Structures

journal homepage: www.elsevier.com/locate/jfs

Rapidly deployable hulls and on-demand tunable hydrodynamics with shape morphing curved crease origami

Hardik Y. Patil [a], Kevin J. Maki [b], Evgueni T. Filipov [a,c,*]

[a] Civil and Environmental Engineering, University of Michigan, Ann Arbor, 48109, MI, USA
[b] Naval Architecture and Marine Engineering, University of Michigan, Ann Arbor, 48109, MI, USA
[c] Mechanical Engineering, University of Michigan, Ann Arbor, 48109, MI, USA

ARTICLE INFO

Keywords:
Curved-crease origami hulls
Tunable hydrodynamics
Shape morphing hulls
Deployable hulls

ABSTRACT

Traditional hull fabrication relies on labor- and time-intensive methods to generate smooth, curved surfaces. These conventional methods often lead to hull surface topologies that are static in design with hydrodynamics aimed at handling a broad range of sea conditions but not optimized for any specific scenario. In this paper, we introduce a method of rapidly fabricating planing hulls using the principles of curved-crease origami. Starting from a flat-folded state, the curved-crease origami hulls can be deployed to match traditional planing hull shapes like the VPS (deep-V, Planing hull with Straight face) and the GPPH (General Purpose Planing Hull). By extension of the ability to conform to a desired shape, we show that the curved-crease origami hulls can emulate desired hydrodynamic characteristics in still as well as wavy water conditions. Furthermore, we demonstrate the shape-morphing ability of curved-crease origami hulls, enabling them to switch between low and high deadrise configurations. This ability allows for on-demand tuning of the hull hydrodynamic performance. We present proof-of-concept origami hulls to demonstrate the practical feasibility of our method. Hulls fabricated using the curved-crease origami principles can adapt to different sea states, and their flat foldability and deployability facilitate easy transport and deployment for rapid response naval operations such as rescue missions and the launch of crewless aquatic vehicles.

1. Introduction

Advanced boat-building and sailing technologies have existed since 6000 BCE (Carter, 2006). Despite the impressive technological strides in naval engineering over centuries, hull fabrication continues to be an enduring and intricate task. Hull fabrication relies on labor-intensive methods that involve connecting numerous flat sheets through bolting, riveting, or welding to form smooth, curved surfaces (Paoli and Razionale, 2012). Achieving the necessary smooth curved surfaces also requires complex casting, milling, and molding procedures. Another challenge is that a significant portion of hull fabrication occurs in landlocked regions, necessitating the transportation of ship parts to coastal docks for assembly (Bruce, 2021). This transportation further extends the construction timeline and associated costs. These current hull fabrication techniques lead to designs with static surface topologies, resulting in hydrodynamics that are a compromise to accommodate a broad spectrum of sea conditions. Consequently, these hulls are not optimized for specific conditions, often leading to inefficient power consumption, poor maneuverability, and reduced passenger comfort and safety. For instance, crew members experience musculoskeletal pain and mental fatigue due to repeated exposure to vertical accelerations caused by the porpoising motion of vessels (de Alwis et al., 2017). These multifaceted challenges underscore

* Corresponding author at: Civil and Environmental Engineering, University of Michigan, Ann Arbor, 48109, MI, USA.
E-mail address: filipov@umich.edu (E.T. Filipov).

https://doi.org/10.1016/j.jfluidstructs.2024.104176
Received 29 March 2024; Received in revised form 16 August 2024; Accepted 26 August 2024
Available online 11 September 2024
0889-9746/© 2024 Elsevier Ltd. All rights are reserved, including those for text and data mining, AI training, and similar technologies.

the need to adopt innovative approaches in the shipbuilding industry, focusing on more versatile fabrication processes and improved adaptability in hull performance.

Origami, the age-old art of paper folding, presents a promising extension to the existing fabrication techniques used by the shipbuilding industry. In recent years, origami has transcended its traditional boundaries and found remarkable applications in engineering structures (Meloni et al., 2021). One key characteristic of origami-inspired structures is their ability to transform flat sheets into complex, three-dimensional structures. This geometrically transformative process dynamically changes the properties of structures and the surrounding fluid media to meet multiple design objectives by varying the extent of folding, as shown by Chen et al. (2023) and Hu et al. (2023). Origami-inspired designs embody several advantageous characteristics, each with unique applications. For instance, structures designed using origami principles can be rapidly deployed from compact configurations and easily reconfigured for various functions (Zirbel et al., 2015). This reconfigurability has potential applications, such as creating stents for minimally invasive surgeries in biomedical engineering (Kuribayashi et al., 2006) and improving the storage and deployment of satellites and solar arrays in space structures (Bowen et al., 2016). Origami principles are also scale-independent (Dudte et al., 2016), making them applicable to structures ranging from deployable stadium canopies to micro-scale sensors. Additionally, the active folding capability enables these structures to change form on demand, increasing their adaptability to various loads and conditions — a strategy often employed by biological organisms to survive in strong winds or water currents (Harder et al., 2004). Thus, incorporating origami principles into ship hull design offers benefits such as flat foldability, efficient storage and transport, and rapid deployment.

While traditional origami surfaces such as Miura-ori (Miura, 2008) are characterized by rough and angular profiles, curved-creasing — a subset of origami, provides a groundbreaking approach to fabricating hull-type structures in naval engineering. Research by Demaine et al. (2011) demonstrates that folding a sheet of material along arbitrary non-intersecting curved creases enables rapid and easy fabrication of smooth curved surfaces. Curved-crease origami preserves the inherent merits of conventional origami techniques while offering numerous benefits suited for hull fabrication. For instance, curved creasing grants precise control over surface topologies by tuning the crease geometry and extent of actuation. Furthermore, it enables the fabrication of complex 3-D shapes that embody benefits such as reduced joint complexity, increased global stiffness, and improved resistance to buckling (Woodruff and Filipov, 2021).

Motivated by the potential of curved-crease origami principles, this study presents an approach for fabricating planing hulls. Planing hulls commonly feature a V-shaped bottom and a transom stern design, which generates hydrodynamic lift to support the hull weight and enable high-speed travel. As a result, these hulls are widely used for applications such as Coast Guard boats, rescue vessels, and ocean racers (Savitsky, 1985). Tavakoli et al. (2024) provides a detailed review of the topology and hydrodynamics of planing hulls. The inherent geometry of planing hulls (see Section 2) makes them an ideal candidate for incorporating curved-crease origami-based fabrication techniques. Thus, as a first step towards curved-crease origami-based hulls, we limit the scope of our exploration to idealized planing hulls. While we agree that extending origami principles to general hull forms poses several challenges at this stage, it still holds significant potential for curved surface fabrication and will be explored separately in the future.

By leveraging the principles of origami, we demonstrate the capability to reproduce a predetermined target planing hull shape with precision. This capability enables the emulation of a desired hydrodynamic behavior and embodies the fabrication efficiency inherent to curved crease origami. Furthermore, through the strategic utilization of active folding in curved-crease origami hulls, we illustrate their ability to undergo a characteristic shape change in real-time. This shape morphing behavior enables on-demand tunability of hydrodynamic properties and renders them applicable across a wide variety of sea conditions. Hulls fabricated using the proposed methods can adapt to any sea state, and their flat foldability and rapid deployment will facilitate easy transport and deployment for naval operations such as covert rescue missions and the launch of crewless decoy marine vehicles. These vehicles will also improve sea-keeping performance, power efficiency, maneuverability, and passenger comfort, making them suitable for civilian recreational use.

The remainder of the manuscript is organized as follows. Section 2 reviews standard planing hull geometries and curved folding procedures. The subsections discuss the planing behavior and typical geometric features of a planing hull, the development of a curved-origami crease pattern for the planing hull, an overview of the numerical model for curved-origami folding, and geometric parameter optimization to match curved-origami hulls to their target shape. Next, Section 3 explores the hydrodynamic analysis of curved-origami planing hulls. The scope of this section is to detail the algorithm used for the hydrodynamic analysis of curved origami planing hulls and the performance evaluation of curved origami planing hulls against target hull shapes. The core findings of this study, including the on-demand shape morphing capabilities of curved-origami hulls and tunable hydrodynamic characteristics for a wide range of sea conditions, are presented in Section 4. A discussion of the key findings, the scalability of origami hulls with an emphasis on curvature analysis for various construction materials and future work is presented in Section 5. Finally, concluding remarks summarizing the key contributions are included in Section 6.

2. Geometry and curved folding

2.1. Planing hull geometry

In a state of rest, buoyant forces are responsible for bearing the weight of a floating hull. Buoyancy is also crucial at lower speed since the hull stays afloat by displacing a volume of water. However, as the speed increases, hydrodynamic lift becomes dominant over the buoyant force and supports the weight of the hull. This hydrodynamic lift allows a planing hull to rise and glide on the water surface.

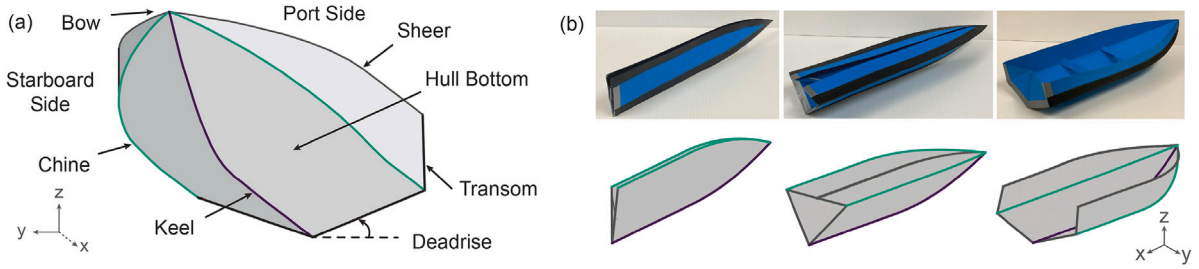

Fig. 1. (a) Geometric features of a typical planing hull: specifically a deep V-shape, Planing hull with a Straight planing surface (VPS); (b) Sequential deployment of curved-crease origami hull designed to match the shape of a VPS hull: paper model (top) compared with Bar and Hinge simulation (bottom). A transom is not included in the simulation.

A typical planing hull has distinct geometric features that enable it to generate hydrodynamic lift. These geometric features of a planing hull (some illustrated in Fig. 1 (a)) can be defined as follows: *(i) Bow*: the foremost part of the hull; *(ii) Chine*: line along which a sharp change in the angle of cross-section occurs; *(iii) Deadrise*: the angle between the bottom of the hull and horizontal surface; *(iv) Draft*: the distance between the waterline and the deepest part of the boat in steady state; *(v) Hull Bottom*: bottom surface of the hull (also called the planing surface); *(vi) Keel*: bottom-most longitudinal structural element of a hull; *(vii) Sheer line*: the uppermost edge of the hull; *(viii) Stern*: the aftmost part of the hull; *(ix) Transom*: the flat board extending from the keel to the deck at the stern; *(x) Trim*: the angle between the horizontal surface and the line connecting the forward and the aft draft; and *(xi) Waterline*: the level water reaches on the hull's side. In some cases, the hull has a parallel section and can be divided into two parts longitudinally, namely the prismatic and non-prismatic sections. The prismatic section often forms the middle to aft half of the hull where the keel and chine lines are parallel. On the other hand, the non-prismatic section forms the front portion of the hull where the keel and chine lines are no longer parallel.

It is important to note that the planing hulls discussed in this paper are hard-chined vessels, which means that the hull exhibits a distinct change of angle along the chine, where the bottom surface meets the sides of the boat. Additionally, these planing hulls feature a typical V-shaped bow with straight surfaces instead of an axe, bulbous, parabolic, or flared bow.

The curved-crease origami-inspired planing hulls offer a method to change some of the aforementioned geometric features that directly affect the hull's planing ability, stability, ride comfort, maneuverability, and power efficiency. Throughout its deployment, the curved crease origami hulls can vary the deadrise, hull length, topology of the curved planing surface, and beam length. The deployment process from a flat-folded to a deployed-hull state is shown in Fig. 1 (b) for both a 20-inch long paper prototype and for a corresponding Bar and Hinge simulation (discussed in the following section). The planing hull design, obtained using the bar and hinge model, is presented here without the transom to reveal distinctive features of the hull, including the chine, keel, and profile of the planing surface. However, the transom can be incorporated into the model, akin to the paper prototype shown in Fig. 1 (b).

2.2. Crease geometry and bar and hinge model for curved folding

A curved crease pattern presented in Fig. 2 (a) is developed to match the VPS hull designed by Kim et al. (2013). VPS stands for deep V-shape, Planing hull with a Straight planing surface, and resembles the shape illustrated in Fig. 1 (a). This crease pattern unfolds into a 3D shape with all the geometric features of a typical planing hull. The geometric parameters used to define this crease pattern are: *(i)* width of the hull's bottom surface between the chine and the keel, H; *(ii)* height of the tip, h_{tip}; *(iii)* overall length of the crease pattern, L_{OA}; *(iv)* length of the prismatic part of the chine, L_P^c; *(v)* length of the non-prismatic part of the chine, L_N^c; *(vi)* length of the prismatic part of the keel, L_P^k; and *(vii)* length of the non-prismatic part of the keel, L_N^k.

The curved portions (non-prismatic section) of the chine and the keel curves are parabolic and denoted by y_c in Eq. (1) and y_k in Eq. (2), respectively. For a given overall length of the crease pattern, the length of the non-prismatic section for the chine and keel curves are denoted by L_N^c in Eq. (3) and L_N^k in Eq. (4), respectively. These quantities can be computed as:

$$y_c = \left[\frac{h_{\text{tip}} - H}{{L_N^c}^2}\right] \times \left(x - L_P^c\right)^2 + H \ , \tag{1}$$

$$y_k = \left[\frac{h_{\text{tip}}}{{L_N^k}^2}\right] \times \left(x - L_P^k\right)^2 \ , \tag{2}$$

$$L_N^c = L_{OA} - L_P^c \ , \tag{3}$$

$$L_N^k = L_{OA} - L_P^k \ . \tag{4}$$

The curved folding simulation of the origami crease pattern into a planing hull shape is accomplished through the Bar and Hinge model developed by Woodruff and Filipov (2020). This model offers a simplified numerical approach that effectively simulates the fundamental behaviors of curved origami folding by employing three distinct elements, as illustrated in Fig. 2 (d). These elements

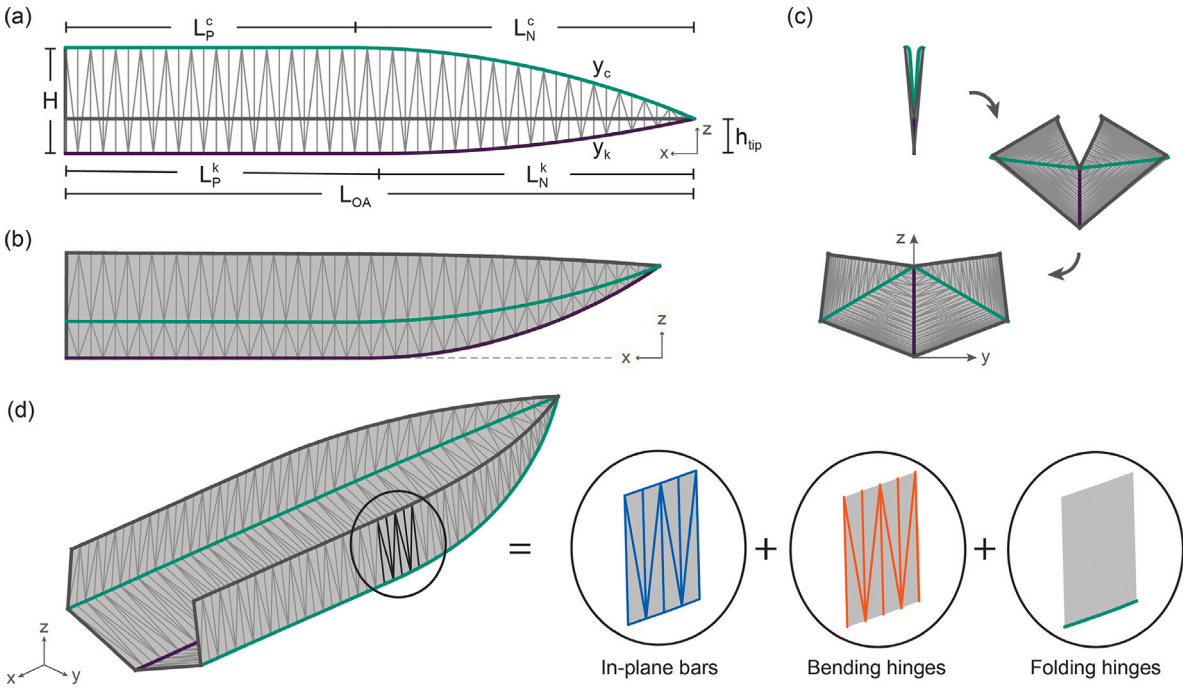

Fig. 2. (a) Geometric parameters defining the curved crease pattern for a planing hull shape; (b) Folded curved-crease origami hull shape viewed from starboard side; (c) Flat, intermediate, and fully folded (clockwise from top) curved-crease origami hull shape viewed from the Transom (also known as Stern) side; and (d) Decomposition of the Bar and Hinge model into its components: in-plane bars, bending hinges, and folding hinges.

can be described as follows: *(i)* three-dimensional truss elements, or bars, that capture in-plane stretching and shearing of the sheet; *(ii)* rotational springs, or hinges, that capture the out-of-plane bending of the sheet by consolidating bending into discrete rotations along the bar lengths; and *(iii)* another set of hinges that capture the rotations at the creases or fold lines.

The crease pattern is meshed using a combination of the three elements, where the stiffness of each element is determined based on material properties, sheet thickness, and mesh size. Despite the inherent geometric nonlinearity involved in the folding process, the model achieves convergence within a short time frame (less than 10 s). This rapid convergence is due to the relatively low number of elements in the Bar and Hinge model compared to finite element methods. Consequently, this rapid simulation enables efficient analysis of curved origami structures, facilitating subsequent shape-matching and optimization processes.

2.3. Shape matching and optimization

The geometric design parameters presented in Fig. 2 (a) can be varied and optimized such that the curved crease origami (CCO) hull shape will match the desired target shape. The matching of CCO hull with target hull shapes is significant for two reasons. Firstly, it enables the reproduction of specific hydrodynamic characteristics by replicating the target shape. Secondly, it facilitates the integration of origami-based design principles in conventional hull design, thereby unlocking the potential to design on-demand shape morphing hulls with tunable hydrodynamics. This section will explore two design variations of the CCO hulls, CCO^{VPS} and CCO^{GPPH}, and compare their shapes with those of the VPS and the General Purpose Planing Hull (GPPH) shapes, respectively.

The quantification of dissimilarity between a CCO hull shape and a target shape is performed using a parameter called the Hausdorff distance, d_H. By definition, the Hausdorff distance represents the maximum distance between any point in one set and the closest point in the other set in three-dimensional space, indicating the largest discrepancy between the two point sets. Hence, smaller Hausdorff distances between two sets (two shapes in this case) indicate a closer match. To ensure consistency in comparing the two different design variants of the CCO hulls with their target shapes, we will represent the Hausdorff distance as the percentage of the overall length, L_{OA} of the hull's planing surface. We specifically emphasize comparing the planing surface because its interaction with water is the predominant factor that influences the hydrodynamic behavior of the hull.

The planing surfaces of CCO^{VPS} and VPS hulls are populated with approximately 5000 points, and the Hausdorff distance for each point on the CCO^{VPS} hull is computed with respect to the VPS hull (Fig. 3 (a)). As the folded shape of the CCO^{VPS} hull is influenced by the geometric parameters of the curved-crease pattern, a simple optimization problem is formulated to find optimal values that minimize the Hausdorff distance between the two hulls. The objective of this problem is to minimize the mean Hausdorff distance between the two hulls, considering the following design variables: *(i)* overall length of crease pattern (L_{OA}), *(ii)* width of the planing panel (H), *(iii)* tip height (h_{tip}), *(iv)* length of the prismatic part of chine (L_P^c), *(v)* length of the prismatic part of the keel (L_P^k), and *(vi)* deadrise of the hull. The optimizer successfully achieves a mean Hausdorff distance of 0.424% and a maximum

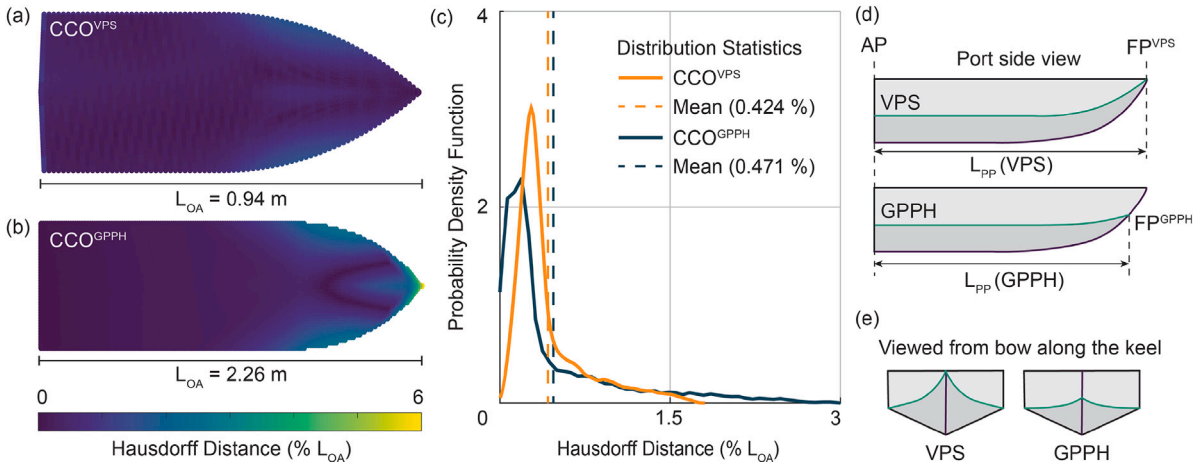

Fig. 3. Color heat map showing the Hausdorff distance as a percentage of the overall hull length (L_{OA}) for the planing surface of two different CCO hull designs compared with: (a) 0.94 m long VPS hull and (b) 2.26 m long GPPH, respectively; (c) Hausdorff distance distribution statistics for CCO hull designs' planing surface compared with corresponding VPS and GPPH designs; (d) Port side view depicting the location of forward perpendicular (FP), aft perpendicular (AP) and the length between the two perpendiculars (L_{PP}); and (e) Bow view when looked along the keel of the VPS and GPPH showing the difference in the chine and keel configuration.

Hausdorff distance of under 2% of the overall length of the hull, indicating an excellent match between the two shapes. This method enables on-demand replication of hull shapes using curved-crease origami principles for innovative hull design and hydrodynamic optimization.

A similar shape-matching procedure is performed for the CCO^{GPPH} and the GPPH hulls with approximately 7500 points. In this case, the mean Hausdorff distance is observed to be 0.471%, and the maximum Hausdorff distance is under 6% of the overall GPPH length. The larger Hausdorff distances compared to the previous case, particularly towards the bow of the hull (see Fig. 3 (b)), can be explained by the difference in the keel extension of the hull designs. As illustrated in Fig. 3 (d) and (e), the keel line of the GPPH extends beyond the chine. Meanwhile, the chine and keel lines of the VPS and both CCO hull designs terminate at the same point on the hull's bow. This difference in keel extension leads to a dissimilar bow shape in the GPPH design compared to the VPS and both CCO hull designs, thus explaining the higher Hausdorff distances.

Despite the minor dissimilarities observed near the bow of the hull in the cases of the VPS and GPPH, the CCO hulls achieve a close match over the prismatic section of the planing surface. The mean Hausdorff distance for the prismatic section of VPS and GPPH equivalent CCO hulls is observed to be 0.258% and 0.281% of the overall length, respectively. Furthermore, the distribution of Hausdorff distances shown in Fig. 3 (c) indicates that the mean Hausdorff distance is less than 0.5% of the overall length for most parts of the planing surface that would interact with water. This similarity in shape and deadrise ensures that the CCO hull can potentially exhibit hydrodynamic characteristics comparable to those of the conventional VPS and GPPH hull designs. Detailed findings related to the hydrodynamic properties and the comparison between the CCO hulls, VPS, and GPPH are presented and discussed in the subsequent sections.

3. Hydrodynamic analysis

The primary purpose of this section is to introduce a hydrodynamic analysis tool, Powersea, capable of carrying out low-cost analyses of various hull shapes. In addition, this section also demonstrates the ability of CCO hulls to match the hydrodynamics of their target shapes (expected because of their highly similar shapes) by explicitly comparing and verifying the Powersea simulation results.

3.1. Powersea: low aspect-ratio strip theory for hull hydrodynamics

The hydrodynamic performance of planing hulls discussed in this study is evaluated using Powersea, a simplified computational tool for rapidly estimating the motion and forces experienced by a hull. Powersea can estimate the heave, pitch, and surge motions of a hull shape, given a forward speed and water conditions, whether still or wavy. Therefore, it enables the investigation of the hull's porpoising behavior for seakeeping ability, effective power requirements, and dynamic natural frequencies in regular and irregular seas. This section explains the theoretical framework behind the low aspect-ratio strip theory algorithm and the underlying assumptions that make Powersea suitable for analyzing CCO planing hulls.

The theoretical framework of Powersea is based on the Low-aspect-ratio strip theory for planing hulls developed by Zarnick (1978, 1979). This theory models the hull motion by discretizing the hull into a series of 2-D strips or wedges. In a water-fixed frame of observation, as illustrated in Fig. 4 (a), these wedges impact the water surface with the progression of time. Fig. 4 (b)

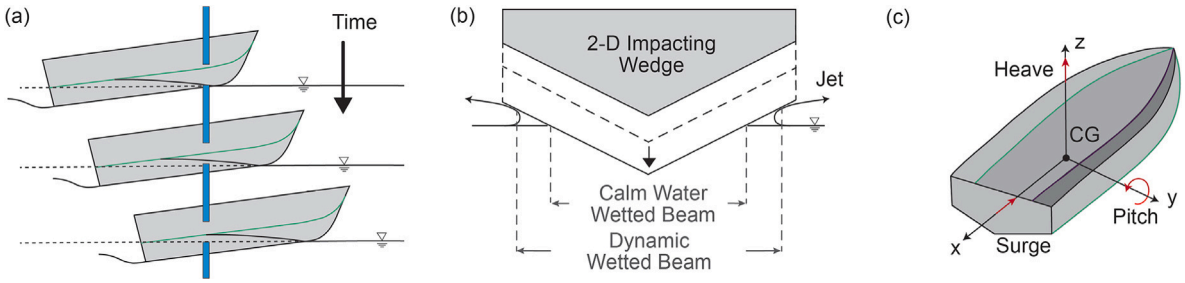

Fig. 4. Graphical representation of the assumptions of Powersea theory: (a) Observation plane indicating the section of the planing hull interacting with the water surface with the progression of time; (b) A single wedge impacting vertically on the water surface; (a) & (b) adapted from Barry et al. (2002); (c) Significant DOFs: Heave (η_3) — translation along the Z-axis, Pitch (η_5) — rotation about the Y-axis, and Surge (η_1) — translation along the X-axis.

depicts a single wedge impacting the water surface and the assumptions used to calculate its hydrodynamic force per unit length. The total hydrodynamic forces acting on the hull body are then obtained by integrating the strip-wise hydrodynamic forces over the instantaneous wetted length of the hull. The 2-D strip theory makes three simplifying assumptions to reduce the number of active degrees of freedom of the hull and the total computational time as compared to a traditional full-scale computational fluid dynamics diffraction-radiation model. First, it is assumed that the perturbation velocities due to straight-line motion are considerably smaller in comparison to the velocity of the hull. Therefore, simplifying the equations of motion by setting the forward velocity of the hull to a constant. Second, only the vertical plane's force and pitch moment excitation are considered while formulating the equations of motion for each wedge, thereby reducing the total number of degrees of freedom. Third, the mathematical formulation of fluid flow is an empirical synthesis of theoretically derived flows. While this formulation is not explicit, there is sufficient confidence to expect promising results (Faltinsen and Zhao, 1991; Sun and Faltinsen, 2007; Korobkin et al., 2017). In addition to predicting hull motion and resistance in still water and waves, Powersea generates a longitudinal distribution of forces on the wedges and can be used to estimate pressures acting on the hull surface for the hull's structural integrity analysis. Akers (1999) outlines the details of the analysis procedure, strip-wise integration, solution of equations for Powersea, and a process to estimate sea loads on the planing surface based on Zarnick's formulation.

The assumptions of strip theory impose certain limitations on the hull geometry and hydrodynamics that powersea can simulate. Powersea assumes that the planing hull is hard-chined and has vertically extended sides. Furthermore, although Powersea predicts the heave motion, pitch motion, and calm water resistance accurately, the vertical acceleration of the hull is underpredicted by about 30% in regular and random seas (Akers, 1999) and the total resistance is underpredicted by about 15% due to not considering the whisker spray (Savitsky et al., 2007). Nonetheless, the hydrodynamic properties are repeatable and can be tuned for engineering purposes. The above limitations are not of concern for our study, and in fact, the low aspect ratio strip theory is well suited for simulating origami-inspired planing hulls for the following three reasons. First, curved origami structures exhibit a distinctive change in topology or curved surface at the curved fold line, resembling the characteristics of a hard-chined vessel. Second, since the planing surface is the dominant geometric feature that influences the planing behavior of a hull, the shape or orientation of the side panels becomes less significant. Lastly, the computational simplicity facilitates rapid hydrodynamic simulation of various hull geometries within a short time frame. This capability is beneficial for investigating the relative change in hydrodynamic properties due to the effects of shape change resulting from origami folding. Powersea also assumes that the wavelengths encountered by the hull will be significantly larger than its length (wave slopes will be relatively small), and the hull speeds correspond to beam Froude numbers greater than 1 (that is, the vessel is advancing in semi-planing/planing regimes). These assumptions provide a reasonable approximation for many practical scenarios and ensure the applicability of Powersea for studying planing hulls in realistic water conditions.

3.2. Performance evaluation of curved-crease origami hulls

The ability of curved-crease origami (CCO) hulls to align congruently with target hull shapes motivates a comparative investigation to evaluate whether their hydrodynamic characteristics also match those of the conventional hulls. This section compares the hydrodynamic performance of the two distinct CCO hull variants, CCO^{VPS} and CCO^{GPPH} as introduced in Section 2.3, with their corresponding target hull forms, namely the VPS and the GPPH. The hydrodynamic evaluation for all four hull geometries is facilitated by the Powersea tool and encompasses the simulation of hull motion in both still and wavy water (head sea) conditions. The geometric and physical characteristics of the hulls passed as input to Powersea can be found in Table 1.

The still water simulations for all four hull shapes are conducted for various constant speed cases. For the VPS and CCO^{VPS} hulls, these speeds range from 2 to 15.5 m/s. For GPPH and CCO^{GPPH} hulls these speeds range from 2.5 to 20.5 m/s. The speeds correspond to beam Froude numbers, F_B ranging from 1 to 9 for each of the four hull geometries. The beam Froude number is calculated as $F_B = U/\sqrt{g \times B}$, where U is the speed, g is the acceleration due to gravity and B is the beam width (distance between the two chines at transom). Other simulation parameters adhered to the default values specified by Powersea, and the hydrodynamic characteristics are shown in Fig. 5. The hydrodynamic characteristics include: *(a)* friction drag experienced by the hull due to the

Table 1
Geometric and physical characteristics of the hulls for hydrodynamic simulations.

Hull geometry	L_{OA} (m)	L_{PP} (m)	LCG (% L_{OA})	VCG (m)	K_{yy} (% L_{OA})	Weight (N)	B (m)
CCO^{VPS}	0.94	0.92	62	0.056	25	65	0.312
VPS	0.94	0.92	62	0.056	25	65	0.308
CCO^{GPPH}	2.26	2.26	62	0.097	25	995.51	0.583
GPPH	2.26	2.23	62 (% L_{PP})	0.097	25 (% L_{PP})	995.51	0.615

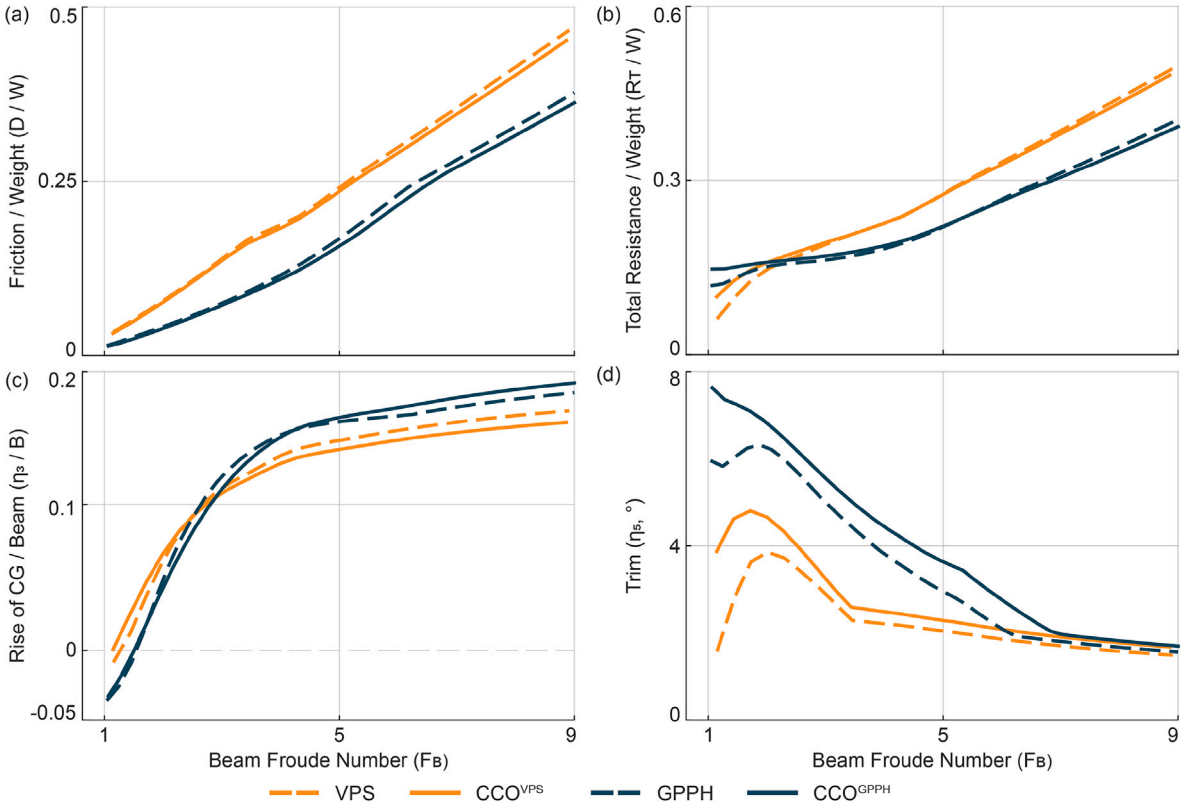

Fig. 5. Comparison of VPS and GPPH hydrodynamics with their CCO counterparts in calm water: (a) Weight normalized friction drag; (b) Weight normalized total resistance; (c) Beam normalized rise of CG; and (d) Trim angle (positive bow up).

shearing of the fluid boundary layer normalized by the hull weight, *(b)* total resistance — a combination of friction drag, viscous pressure drag and wave making resistance, normalized by the hull weight, *(c)* Rise of Center of Gravity (CG) — heave displacement relative to at-rest position normalized by the beam width, and *(d)* trim — running angle of the hull about its lateral axis as it makes way in the water. While the friction drag, rise of CG, and pitch data are generated by Powersea, the weight normalized total resistance, R_T/W, is calculated as follows:

$$\frac{R_T}{W} = \tan(\eta_5) + \frac{D}{W} \times \frac{1}{\cos(\eta_5)}\ , \tag{5}$$

where D is the friction drag, W is the weight of the hull, and η_5 is the pitch (trim angle) (Doctors, 1985). It is important to note that the total resistance does not include whisker spray drag.

It is essential to note that the comparative analysis of CCO hulls with counterparts GPPH and VPS hulls reveals a consistent trend across various hydrodynamic characteristics. Both friction drag in Fig. 5 (a) and total resistance in Fig. 5 (b) exhibit a monotonically increasing trend as the planing speed increases. Additionally, the hull tends to rise on the water surface with an increase in planing speed, as evidenced by the rise in CG illustrated in Fig. 5 (c). Contrarily, the trim angle of the hull diminishes with an increase in the planing speed, as indicated in Fig. 5 (d). However, it is also imperative to acknowledge a slight disparity in the trim angle of the CCO hulls and their GPPH and VPS counterparts. The following reasons can explain this disparity. First, despite exhibiting a close match, the CCO hulls are not identical in shape to their GPPH and VPS counterparts. The minor differences in the shapes of planing surfaces and beam widths, as documented in Section 2.3 and Table 1, respectively, explain the deviations observed in sinkage and the trim angle at various speeds. Second, Powersea requires the forward perpendicular (FP) to be set at the intersection

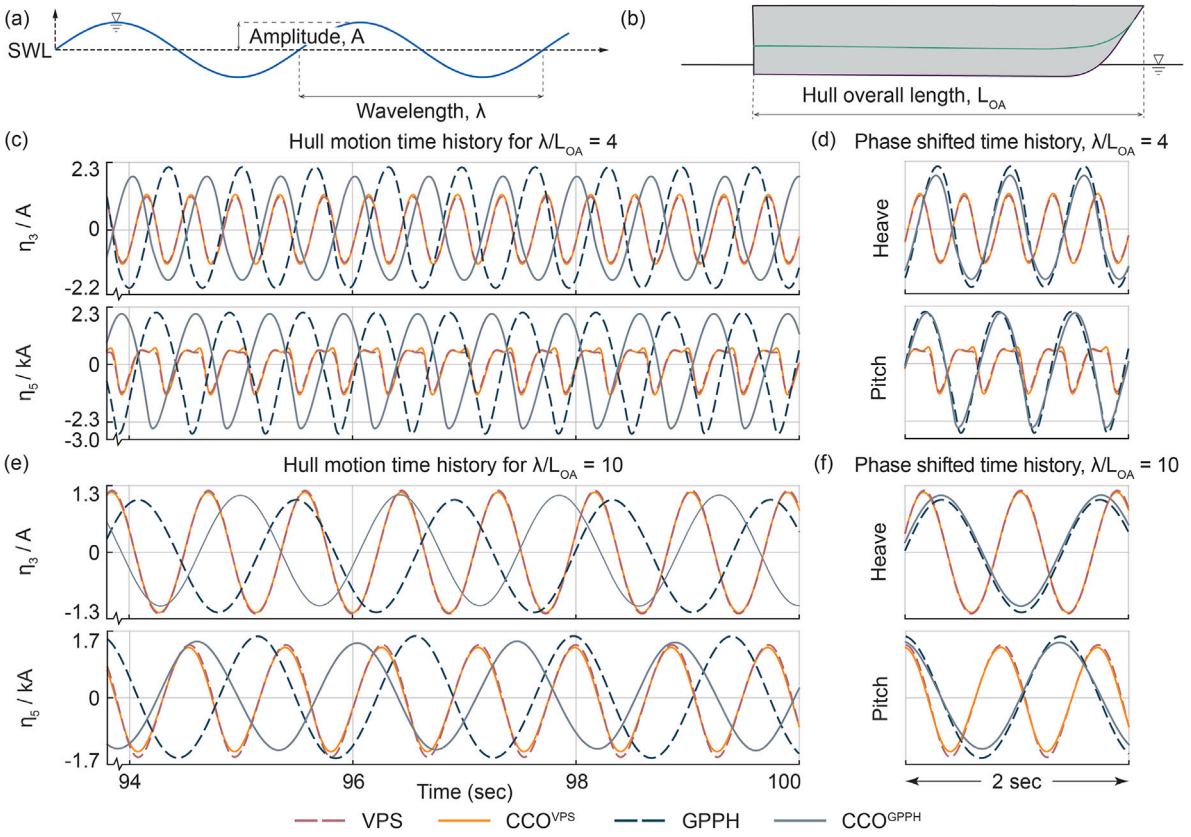

Fig. 6. (a) Regular wave characteristics from a nominal Sea Water Level (SWL); (b) Overall length of the boat; Comparison of mean subtracted VPS and GPPH hull motion time histories with their CCO counterparts in head seas: (c) Six seconds of steady state time history for $\lambda/L_{OA} = 4$; (d) Phase shifted steady state time history over 2 s interval for $\lambda/L_{OA} = 4$; (e) Six seconds of steady state time history for $\lambda/L_{OA} = 10$; and (f) Phase shifted steady state time history over 2 s interval for $\lambda/L_{OA} = 10$. η_3/A is heave normalized by wave amplitude. η_5/kA is pitch normalized by wave slope.

of the chine and keel lines along the hull's length. For both CCO^{GPPH} and GPPH, this requirement results in differing hull length (L_{PP}) between the aft perpendicular (AP) and the forward perpendicular (FP), as shown in Fig. 3 (d). Furthermore, Powersea only utilizes the portion of the hull geometry between the AP and FP to simulate its behavior in water. To ensure consistency across all simulations, we align the FP for all hull geometries with the origin at time t=0. Specifically for the GPPH, the LCG and K_{yy} are set based on the modeled length of the hull which corresponds to (L_{PP}) rather than (L_{OA}) (see Table 1), resulting in a slightly different LCG location compared to CCO^{GPPH}. These modeling differences lead to varying initial equilibrium positions of the hulls and, consequently, to the differences in the trim angle at various speeds. Lastly, the assumptions in Powersea's underlying theory make it less accurate for predicting hull motion in semi-planing regimes and when the beam Froude numbers are less than or equal to 1. Therefore, the significant deviation in the trim angle at lower speeds can be safely disregarded. At high speeds, when the hulls are advancing in the planing regime, and the bows of the hulls are no longer in contact with the water, the CCO hulls and their counterparts exhibit similar performance.

The investigation of hull motion in waves is carried out under constant speed, corresponding to a beam Froude number, $F_B = 4$ when navigating head seas. For VPS and CCO^{VPS} hulls, the speed equals 7 m/s, whereas for GPPH and CCO^{GPPH} hulls, the speed equals 10 m/s. Wave amplitudes of 0.02 m were applied to the VPS and CCO^{VPS} hulls, based on the tank test parameters for VPS hull from the Kim et al. (2013) study. The GPPH and CCO^{GPPH} hulls were subjected to wave amplitudes of 0.04 m to maintain a wave amplitude to hull length ratio similar to that of the VPS and CCO^{VPS} hulls. Each of the four hull geometries was subjected to regular waves with wavelengths, λ equivalent to 4 and 10 times the overall length, L_{OA} of the planing hull. The graphical representation of these regular wave characteristics is provided in Fig. 6 (a) and (b). Fig. 6 (c) and (e) display the final 6 s of the 100-second long time histories depicting the steady state, mean-subtracted heave (normalized by wave amplitude) and pitch (normalized by wave slope) motions of the hulls, corresponding to the non-dimensionalized wavelength represented as λ/L_{OA} ratios of 4 and 10, respectively. The mean values of normalized heave and pitch time histories for all hull geometries and λ/L_{OA} ratios are presented in Table 2. The small differences in the mean values stem from the variations in hull geometry and the modeling methods, as outlined earlier.

The primary objective of these simulations was to acquire a deeper understanding of the similarities and differences in the hull motion of CCO hulls and their counterparts when subjected to waves. It is observed that the oscillatory hull motion for the GPPH and CCO^{GPPH} exhibits a significant phase shift. Nevertheless, the amplitudes and frequencies of the motion are nearly identical when

Table 2
Mean values of the normalized heave and pitch from Fig. 6.

Hull geometry	Normalized mean heave, $\overline{\eta_3}/A$		Normalized mean pitch, $\overline{\eta_5}/kA$	
	$\lambda/L_{OA} = 4$	$\lambda/L_{OA} = 10$	$\lambda/L_{OA} = 4$	$\lambda/L_{OA} = 10$
CCO^{VPS}	2.846	2.127	2.252	3.354
VPS	2.807	2.199	1.933	2.988
CCO^{GPPH}	2.085	2.273	2.741	6.778
GPPH	2.788	2.494	2.854	5.939

Table 3
Geometric parameters of the variable deadrise CCO hulls for hydrodynamic simulations.

Hull geometry (deadrise)	L_{OA} (m)	L_{PP} (m)	LCG (% L_{OA})	VCG (m)	K_{yy} (m)	Weight (N)	B (m)
10°	0.889	0.879	58.76	0.08	0.574	89.3	0.319
20°	0.945	0.935	60.53	0.096	0.623	89.3	0.304
30°	0.962	0.952	61.12	0.097	0.639	89.3	0.278

evaluating the mean and phase-shifted data in Fig. 6 (d) and (f). This phase shift in hull motion can be explained by the modeling differences arising from the variations in L_{PP} and keel configurations between the GPPH and CCO^{GPPH} hull designs. In Powersea, the initial wave trough is positioned at the origin and coincides with the hull's FP at time t = 0. Because the L_{PP} differs between the GPPH and CCO^{GPPH}, the LCG is located differently along each hull's length. This difference results in varying initial equilibrium positions and causes the hulls to encounter waves at different times at the same longitudinal position along the hull. The CCO^{GPPH} has an initial draft of 0.153 m and an initial trim of 4.389°. On the other hand, the GPPH has an initial draft of 0.150 m and an initial trim of 3.862°. Thus, the combined effects of the bow shape influencing the initiation of motion in wavy conditions, the differing initial equilibrium position of the hulls, and the time difference in wave encountered at the same longitudinal position along the hulls' length explain the phase shift between the motion histories of GPPH and CCO^{GPPH} hulls.

In contrast, for the VPS and CCO^{VPS} hulls, we observe no phase shift and nearly identical amplitude and frequency of the motion response for both λ/L_{OA} ratios, as shown in Fig. 6 (c–f). It is important to note that for the λ/L_{OA} ratio of 4, high amplitudes of heave and pitch motion are observed in all four hull geometries, indicating that a wave with λ/L_{OA} ratio of 4 excites the hulls more than a wave with λ/L_{OA} ratio of 10.

The findings from this section offer substantial evidence supporting the ability of CCO hulls to emulate the performance of their target hull shapes in both still and wavy water conditions.

4. Tunable hydrodynamics with shape morphing curved-origami hulls

The curved-crease origami planing hull undergoes a gradual transformation from a flat sheet into the characteristic planing hull shape throughout its deployment. By controlling the resting angle of the fold lines located along the chine and keel of the curved-crease origami hull, we gain the ability to morph the hull shape on demand. This ability allows us to change the hull deadrise and grants control over various other geometric attributes, such as the overall length, beam width, bow curvature, center of gravity location, and the radius of gyration. These parameters collectively exert a significant influence on the hydrodynamic characteristics, allowing for on-demand shape morphing and tunability of hull hydrodynamics.

Here, we first discuss the influence of the rest angle of the fold lines on the hull deadrise and the overall hull geometry, which subsequently affects the hydrodynamic behavior. We will study three distinct hull configurations, all obtained from a single curved-crease pattern (starting configuration of flat sheets). As a starting point, we use the same curved-crease pattern as that developed for the VPS hull. The specific folded configurations correspond to deadrise angles of 10°, 20°, and 30° respectively, as graphically depicted in Fig. 7. A noticeable trend emerges as the hull's deadrise undergoes a transition from 10° to 30°. Specifically, this transition is marked by the following changes: an increase in the hull's overall length, a decrease in the beam width, a reduction in the bow's curvature, a forward displacement and vertical ascent of the center of gravity, along with an accompanying increase in the radius of gyration. In order to assess the influence of this morphable hull shape on the hull's hydrodynamic behavior, a series of simulations were conducted using the Powersea software in both calm waters and head seas. The geometric parameters that served as an input for these simulations corresponding to each configuration are presented in Table 3.

4.1. Calm water hydrodynamics

The simulations in still water for all three curved-crease origami hull configurations are conducted for various constant speed cases. The speeds (2 to 15.5 m/s) correspond to beam Froude numbers, F_B ranging from 1 to 9 for each of the three hull geometries. All simulation parameters adhere to the default values specified by Powersea, and the hydrodynamic characteristics are presented in Fig. 7. Similar to the preceding hydrodynamic investigation conducted in calm water, the attributes studied within this context include: *(a)* friction drag normalized by the hull weight, *(b)* total resistance normalized by the hull weight, *(c)* rise of CG normalized by the beam width, and *(d)* trim angle of the hull.

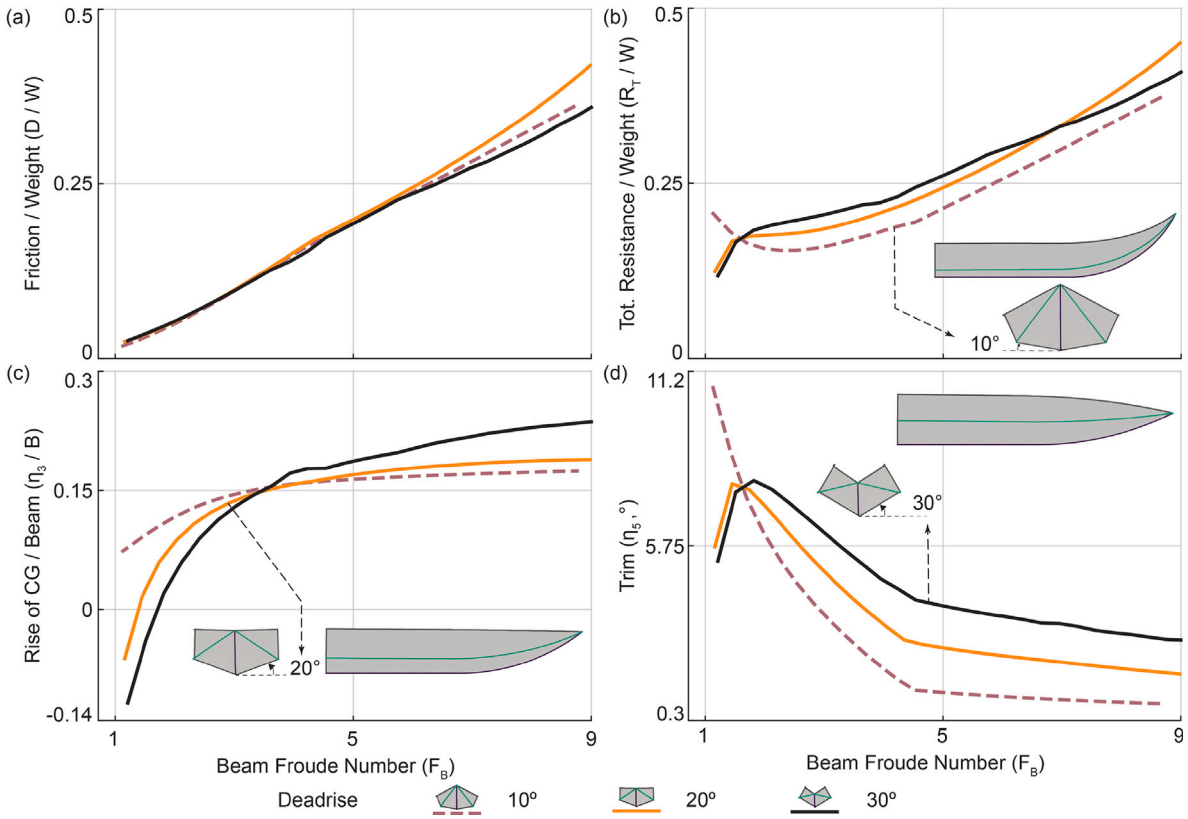

Fig. 7. Effect of varying the CCO hull's deadrise on hydrodynamic performance in calm water: (a) Weight normalized friction drag; (b) Weight normalized total resistance; (c) Beam normalized rise of CG; (d) Trim angle (positive bow up).

The influence of shape change on the weight-normalized friction drag experienced by the hull across all deadrise variations is insignificant, except at very high speeds. As illustrated in Fig. 7 (a), the 20° deadrise hull exhibits slightly higher frictional resistance than 10° and 30° deadrise configurations at F_B close to 9. For a lower deadrise configuration, there is an increase in the total resistance at lower speeds, but an interesting reversal of trends emerges at higher speeds. As seen in Fig. 7 (b), the lower deadrise configuration now exhibits lower total resistance. A similar trend is also observed for the trim angle of the hull, as shown in Fig. 7 (d). This change in trends for total resistance is expected because it is a derived quantity that depends upon the friction drag and trim angle. Since friction drag shows little variation across deadrise configurations, the trend of trim angle contributes to that of the total resistance. In the case of rise of CG, the low deadrise configuration tends to rise higher than the high deadrise configurations for F_B up to 4, as shown in Fig. 7 (c). A noticeable reversal in the hull rise trend emerges at high speeds. The variation in hull rise remains negligible across all deadrise configurations for practical considerations with the exception of the 30° deadrise configuration. These results can be interpreted in the following ways. In the case of a curved-crease origami hull configured with a lower deadrise, the planing surface typically takes on a flatter and broader profile. Consequently, with increasing surge speed, the hull tends to rise and glide over the water's surface. This phenomenon results in a reduced trim angle as the hull does not have to plow through the water, thereby leading to lower total resistance. In contrast, for a curved-crease origami hull configured with a higher deadrise, the planing surface is generally a shaper V shape with a narrower profile. This hull tends to sink deeper into the water. Consequently, this hull has to overcome greater total resistance and exhibits increased trim angle at higher surge speeds.

4.2. Wavy water hydrodynamics

The investigation of hull motion in waves is carried out under the condition of a constant speed of 4.04 m/s when navigating head seas. The speed corresponds to F_B of 2.28, 2.34, and 2.44 for the 10°, 20°, and 30° deadrise configuration, respectively. Wave amplitudes of 0.02 m are applied to all three hull geometries. Each of the three hull geometries is subjected to regular waves with wavelengths equivalent to 4, 8, and 12 times the overall length of the planing hull. The mean subtracted steady-state hull motion is depicted in Fig. 8 (a–c). These figures display the final 10 s of the 100-second time histories and illustrate the heave normalized by wave amplitude and pitch normalized by wave slope of the hulls for the three λ/L_{OA} ratios.

The objective here is to understand the effects of varying deadrise configurations of the curved-crease origami hull on its performance under different wavy conditions. We observe that the hull configured with 30° deadrise exhibits strikingly smaller

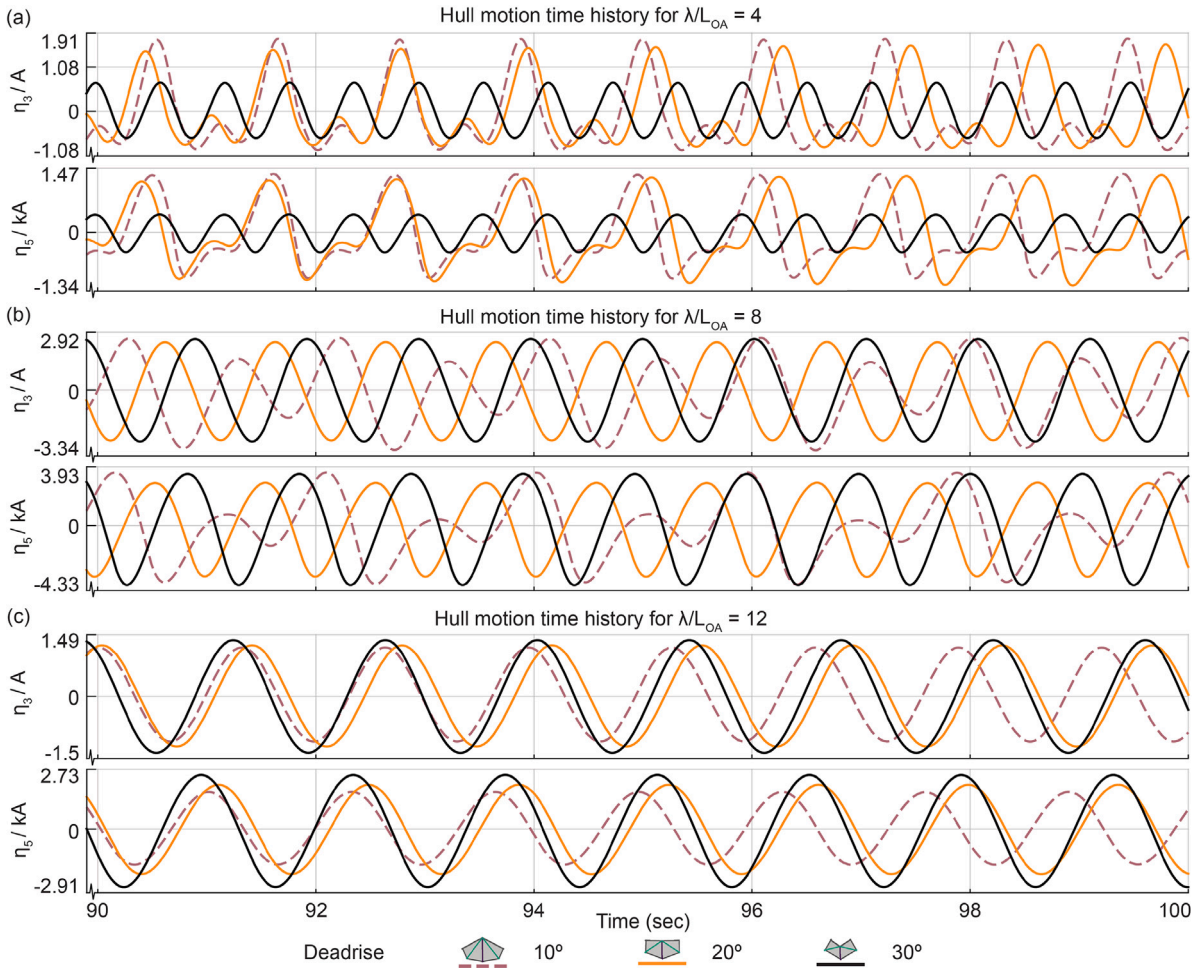

Fig. 8. Effect of varying the CCO hull's deadrise on steady state hull motion in head seas for: (a) $\lambda/L_{OA} = 4$; (b) $\lambda/L_{OA} = 8$; (c) $\lambda/L_{OA} = 12$. Surge speed is 4.04 m/s, wave amplitude is 0.02 m and the last 10 s of the mean subtracted hull motion time history is shown. η_3/A is heave normalized by wave amplitude. η_5/kA is pitch normalized by wave slope.

heave and pitch amplitudes for the λ/L_{OA} ratio of 4 compared to other configurations. As the λ/L_{OA} ratio increases to 8, the heave and pitch amplitudes increase for all hull shapes. Next, at λ/L_{OA} ratio of 12, there is a decrease in the motion amplitudes. The hull configured with 10° deadrise exhibits non-monochromatic hull motion, with higher amplitudes at shorter wavelengths, but reduces in amplitude and becomes monochromatic as the exciting wavelength increases. This hull shape has substantially higher amplitudes at shorter wave frequencies (i.e. $\lambda/L_{OA} = 4$), which can be expected for planing hulls with lower deadrise angles (flatter hull surface). Our observation here underscores the profound implications of altering the curved-crease origami hull's deadrise configuration on hull motion and overall hydrodynamics. Consequently, the shape-morphing ability of the hull can be harnessed to tune the hull response on-demand, making a single hull geometry adaptable to a wide range of sea conditions.

5. Discussion

5.1. Key findings

Using reduced-order numerical simulations for curved origami folding and hydrodynamic analysis, we have explored the versatility of curved-crease origami hulls. In particular, the study has demonstrated the following advantages associated with curved-crease origami hulls.

Rapidly deployable hulls that start as flat sheets and conform to desired shapes. The curved-crease origami hulls introduced in this study can be designed to conform to a desired hull shape by adjusting and optimizing the geometric parameters of the initial curved-crease pattern. Shape-matching analysis reveals that these hulls exhibit a mean Hausdorff distance of less than 0.5% of the overall hull length across much of the planing surface that would interact with water. Consequently, traditional hull designs like

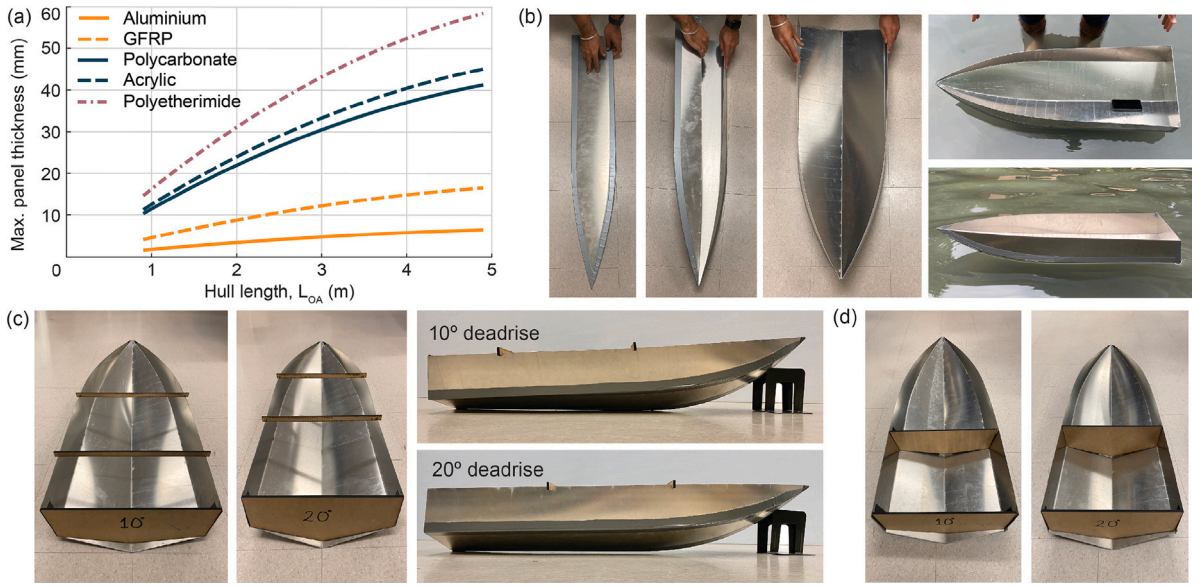

Fig. 9. (a) Scalability analysis demonstrating the elastic limit (maximum thickness) for curved-crease origami hulls for different materials; (b) A 91 cm (36 in.) long curved-crease origami hull prototype fabricated using 1.5 mm thick aluminium sheets, joined together with duct tape for flexible joints — displaying the stowed (left) to deployed (right) configuration; (c) Aluminium CCO hull configured with deadrise configurations 10° and 20° strengthened with lateral stiffeners that snap onto the side of the hull; (d) Aluminium CCO hulls fitted with solid bulkhead.

the VPS (deep-V, Planing hull with Straight surface) can be fabricated using curved-crease origami techniques. Despite being non-developable, the entire curved-crease origami hull can be fabricated in a flat-folded state. This flat-foldability presents advantages over conventional fabrication methods, such as facilitating off-site construction and efficient storage and transportation. Moreover, the curved-crease origami hulls can be deployed rapidly from their flat folded state. This attribute is particularly advantageous in scenarios such as post-disaster relief operations for search and rescue, as well as the deployment of multiple uncrewed aquatic vehicles for naval operations, where prompt response, multiple distributed vessels, and adaptability are paramount.

Replicating hydrodynamics of conventional hull forms. By extension of the ability to conform to conventional hull shapes, the curved-crease origami hulls demonstrate hydrodynamic performance that closely matches their conventional counterparts (VPS and GPPH). The hydrodynamic simulations performed with Powersea in still water conditions reveal nearly equivalent trends in performance characteristics such as friction drag, total resistance, hull sinkage, and trim over a wide range of forward speeds. In wavy water (head seas) conditions, the curved-crease origami hulls demonstrate a notable similarity in the amplitude and frequency of the hull motion time histories to their conventional counterparts. These observations suggest that hulls designed with curved origami principles can be expected to deliver comparable performance to the traditional hulls, that is, maintain power efficiency, passenger comfort, and safety, among other performance parameters, in addition to the inherent advantages offered by origami fabrication techniques.

Shape morphing hulls for on-demand tunable hydrodynamics. Hulls designed with curved origami principles grant control over the angle of the fold lines along the keel and chine of the hull. The extent of folding (or actuation) of these fold lines facilitates on-demand morphing of the hull shape, allowing for the modification of key geometric features, such as the deadrise angle. Notably, hulls configured with a lower deadrise exhibit a flatter planing surface, making them well-suited for calm water conditions. They typically maintain lower sinkage and trim angles, allowing them to experience lower resistance and thus achieve more efficient motion. However, this configuration experiences increased amplitudes of hull motion in waves, making it less suitable for effective seakeeping in wavy conditions. Conversely, the same hull configured with a higher deadrise angle features a sharp V-shaped planing surface. While this configuration typically encounters higher total resistance, sinkage, and trim angles in still waters, the amplitude of hull motion is significantly lower in wavy water conditions compared to their low deadrise counterparts. Thus, a singular curved-crease origami hull can transition between various deadrise configurations, rendering it suitable for use in various sea conditions. Furthermore, tuning its hydrodynamic performance also ensures increased passenger comfort and operational efficiency.

5.2. Physical implementation

Translating these designs into practical, life-sized vessels offers several challenges. Critical consideration must be given to selecting appropriate materials for the panels and the flexible joints to ensure the hull's durability while meeting the demands of the naval industry. A preliminary examination of sheet curvature was conducted to identify suitable material options for curved origami panels. Deforming an initially flat sheet to conform to the curved-crease geometry generates significant bending stresses in the sheet itself. These bending stresses can be used to compute a maximum allowable thickness for the sheet, below which the

material would remain elastic. The following formula was used to determine the maximum allowable sheet thickness for a given material to fabricate a curved crease origami hull: $t = 2\sigma_y/E\kappa$. Here, t represents the maximum sheet thickness, σ_y corresponds to the material's yield strength, E denotes the material's Young's modulus, and κ signifies the maximum sheet curvature, obtained from the Bar and Hinge model for a given length of the curved-crease origami hull. Fig. 9 (a) graphically depicts the maximum permissible sheet thickness for various materials, such as Aluminium, Glass fiber-reinforced polymer (GFRP), Polycarbonate, Acrylic, and Polyetherimide (Ultem®). This analysis, thus, serves as a crucial reference point for material selection and design considerations in fabricating the curved-crease origami hull.

A scaled model of the curved-crease origami planing hull is constructed by leveraging the results of the curvature analysis. Fig. 9 (b) showcases a 91 cm (36 inch) long prototype afloat in a water pond, with a smartphone serving as a reference scale. This prototype is constructed using 1.5-millimeter-thick panels of 6061-grade aluminium. The aluminium panels are connected using heavy-duty duct tape along the curved creases, thus serving as the curved-origami fold joints. This prototype serves as an initial proof-of-concept demonstrating the material selection for prototypes to remain elastic. While simplistic, the joints of our prototype are watertight and allow for multiple fold-unfold cycles without degradation.

Post-deployment, the curved crease origami hulls require reinforcement to prevent collapse and torsional deformations. In Fig. 9 (c), we present the same aluminium CCO hull from Fig. 9 (b), but configured with two distinct deadrise angles — 10° and 20°. Each deadrise configuration is fortified with snap-fit lateral stiffeners, or girders, constructed from a mid-density fiberboard. These stiffeners effectively prevent collapse and provide sufficient reinforcement against torsional deformations, working in conjunction with the stiffness provided by the transom and curved aluminium sheets. The CCO hulls can also be fitted with solid bulkheads, as shown in Fig. 9 (d). In the future, the curved-crease origami hulls can be fitted with deployable bulkheads and stiffeners to strengthen the hull post-deployment.

A parallel fabrication effort is being led by the research team at the Naval Surface Warfare Center, Carderock Division (NSWCCD) for a desktop-scale curved-crease origami-based planing hull with details anticipated to be available publicly soon (Kelly and Hart, Personal Communication, 2024).

5.3. Considerations for future work

Several items remain unexplored, particularly concerning the material selection, actuation methods, the structural integrity of the hull, and an in-depth exploration of the interplay between origami hull shape morphing and hydrodynamics. Future work could focus on:

Optimizing material selection for curved panels and fold joints. Curved-crease origami panels and fold joints experience large strains throughout their deployment process. In addition to the large strains, panels and creases of deployable structures are vulnerable to damage due to long-term storage and fatigue as they underdo repeated folding and unfolding (Ma et al., 2024). In CCO hulls, fatigue-induced cracks can compromise the hull's watertightness, posing a risk of sinking.

To fabricate multi-use deployable curved-crease origami hulls, it is essential to identify flexible materials that can withstand numerous bending and folding cycles while demonstrating durability and resistance to the corrosive marine environment. Current deployable structures with highly deformable components like rigid-hull inflatable boats (Halswell et al., 2011) and pneumatic floats for inflatable bridges (Russell et al., 2014) use materials like Hypalon® coated polyester, PVC, or Polyurethane, which last for 15–20 years before showing signs of damage. Recent work has also highlighted the potential of flexible and durable connections for origami systems using carbon fiber-reinforced polymer and urethane composites (Deleo et al., 2020, 2018). While the proof-of-concept prototypes in Section 5.2 present initial feasibility, future work must focus on: *(a)* the selection of flexible composite materials that are resilient to fatigue damage and *(b)* advanced bonding methods to connect creases and panels. The ongoing work on CCO hull fabrication at NSWCCD (Kelly and Hart, Personal Communication, 2024) also aims to address the issue of fatigue in origami creases by developing cast-in-place neoprene joints for the CCO panels.

Actuation methods and structural stiffeners for enhanced stability. Future research should explore actuation methods for efficiently deploying curved crease origami hulls. Depending on the hull's material, size, and intended application, an investigation of the forces required to transform the hull from a flat-folded to a deployed state must be undertaken. Analysis of the required actuation forces will guide the selection of deployment methods for curved-crease origami hulls (for example, mechanized devices, inflatable systems, or deployment by hand).

The post-deployment strengthening of the CCO hulls is an equally essential area for future exploration. Although we have presented a proof-of-concept in Section 5.2 for the inclusion of stiffeners, future work must focus on: *(a)* incorporating deployable bulkheads, girders, or frames for post-deployment stiffening of the CCO hulls, *(b)* exploring connectors that ensure compatible kinematics between the CCO hull shell and deployable stiffeners and *(c)* studying the quantitative increase of structural stiffness provided by the stiffeners against shell collapse and torsional deformations.

Evaluating structural integrity for various payloads under wave impact loading. A critical area of consideration for curved-crease origami hulls is the evaluation of their structural integrity when subjected to dynamic wave impact loads. Planing hulls are known to experience high pressures locally in the bow area. It is, therefore, essential to assess the local strength of the hull shell, mainly when the thickness of the hull is limited by surface curvature (as shown in Fig. 9 (a)). Thus, future work must study the effects of varying payloads on the pressures and forces experienced by an origami hull in different deadrise configurations. This study could be performed using tow tank tests or CFD hydrodynamic analysis to evaluate pressures and forces on the hull surface and subsequently using structural finite elements analysis to evaluate the structural response, including stresses and strains.

In-depth exploration of the relationship between shape morphing and hydrodynamics. The shape morphing ability of curved-origami hulls not only influences the hull deadrise but also alters various geometric parameters such as the overall length, bow curvature, beam width, center of gravity, and radius of gyration. Our work thus far has highlighted the potential of the CCO hulls' shape-morphing ability for the tuning of hull hydrodynamics. However, we have yet to establish the relationship between the combination of these geometrical transformations and hull hydrodynamics. While Powersea is an excellent tool for analyzing planing hulls with minimal computational costs, a significant amount of valuable information is lost due to the underlying assumptions and simplifications of the flow. These simplifications include the reduction of the order from 3D to 2D and linearizing the free surface condition within each time step, among others. Thus, future work must focus on conducting one-way coupled fluid–structure interaction analyses to comprehensively understand the relationship between the CCO shape change and hull hydrodynamics. This relationship can explored in greater detail by examining the Response Amplification Operators (RAOs), such as the heave and pitch transfer functions, for the varying configurations of the CCO hulls subjected to different wavelengths. By analyzing RAOs, we can better understand how CCO shape changes tune parameters like the resonant frequency of the hull. Moreover, these analyses will simulate hull performance with high confidence levels, allowing us to evaluate characteristics such as added wave resistance, whisker spray resistance, and accelerations at various points on the hull to assess the sea-keeping fitness of CCO hulls. Additionally, tank tests may also be performed to support the CFD results.

Addressing the research topics discussed above will help lead to the future implementation of deployable curved-crease origami planing hulls with on-demand performance tunability and optimization of crew comfort for civil and military applications.

6. Concluding remarks

This paper introduces a hull fabrication approach based on curved-crease origami (CCO) principles. Employing the Bar and Hinge model for curved-origami folding and the Hausdorff distance metric, we explored the ability of two CCO hull variants to conform to conventional VPS and GPPH hull shapes. Obtaining conforming designs was achieved by optimizing the geometric parameters of the curved-crease pattern. Next, we demonstrated the ability of CCO hulls to emulate the hydrodynamic performance of conventional hull forms in still and wavy water conditions using the Powersea tool. Finally, we explored the shape-morphing ability of CCO hulls, which enables on-demand tunability of hydrodynamic performance to suit diverse sea conditions. Proof-of-concept prototypes are fabricated to demonstrate the feasibility of CCO for creating hulls.

CRediT authorship contribution statement

Hardik Y. Patil: Writing – review & editing, Writing – original draft, Visualization, Validation, Software, Methodology, Investigation, Formal analysis, Data curation. **Kevin J. Maki:** Writing – review & editing, Validation, Supervision, Methodology. **Evgueni T. Filipov:** Writing – review & editing, Validation, Supervision, Resources, Project administration, Methodology, Funding acquisition, Conceptualization.

Declaration of competing interest

The authors declare the following financial interests/personal relationships which may be considered as potential competing interests: Evgueni Filipov reports financial support was provided by Office of Naval Research. If there are other authors, they declare that they have no known competing financial interests or personal relationships that could have appeared to influence the work reported in this paper.

Data availability

Data will be made available on request.

Acknowledgments

We acknowledge support from the Office of Naval Research (ONR), USA in the form of a grant (N00014–20–5–B001 #13209604) to Dr. Evgueni T. Filipov. We also acknowledge Daniel Hart and Jason Kelly at Naval Surface Warfare Center, Carderock Division (NSWCCD) for the many helpful discussions related to this project.

References

Akers, R.H., 1999. Dynamic analysis of planing hulls in the vertical plane. In: Proceedings of the Society of Naval Architects and Marine Engineers. New England.

Barry, C.D., Ghosh, D., Akers, R., Ulak, A., 2002. Implementation, application and validation of the zarnick strip theory analysis technique for planing boats. In: Proceedings of High Performance Yacht Design Conference, No. P2002–7. Auckland, New Zealand.

Bowen, L., Trease, B., Frecker, M., Simpson, T., 2016. Dynamic modeling and analysis of an origami-inspired optical shield for the starshade spacecraft. In: Smart Materials, Adaptive Structures and Intelligent Systems, vol. 50480, American Society of Mechanical Engineers, p. V001T01A012.

Bruce, G., 2021. Ship construction. Shipbuild. Manag. 153–162.

Carter, R., 2006. Boat remains and maritime trade in the Persian Gulf during the sixth and fifth millennia BC. Antiquity 80 (307), 52–63.

Chen, G., Chen, D., Weakly, J., Sung, C., 2023. Drag coefficient characterization of the origami magic ball. In: ASME International Design Engineering Technical Conferences and Computers and Information in Engineering Conference. IDETC/CIE.

de Alwis, M., Garme, K., Lo Martire, R., Kåsin, J., Äng, B., 2017. Crew acceleration exposure, health and performance in high-speed operations at sea. In: The 11th Symposium on High-Speed Marine Vehicles. Naples, Italy.

Deleo, A.A., O'Neil, J., Yasuda, H., Salviato, M., Yang, J., 2020. Origami-based deployable structures made of carbon fiber reinforced polymer composites. Compos. Sci. Technol. 191, 108060.

Deleo, A., O'Neil, J., Yasuda, H., Yang, J., Salviato, M., 2018. Composite origami: Foldable structures based on tachi-miura-polyhedron origami technique. In: Proceedings of SAMPE. SAMPE Diamond Bar, CA.

Demaine, E., Demaine, M., Koschitz, D., Tachi, T., 2011. Curved crease folding a review on art, design and mathematics. In: Proceedings of 35th Annual Symposium of IABSE/52nd Annual Symposium of IASS/6th International Conference on Space Structures: Taller, Longer, Lighter — Meeting Growing Demand with Limited Resources. London, United Kingdom, p. 1.

Doctors, L.J., 1985. Hydrodynamics of High-Speed Small Craft. Technical Report.

Dudte, L.H., Vouga, E., Tachi, T., Mahadevan, L., 2016. Programming curvature using origami tessellations. Nature Mater. 15 (5), 583–588.

Faltinsen, O., Zhao, R., 1991. Numerical predictions of ship motions at high forward speed. Philos. Trans. R. Soc. Lond. Ser. A 334 (1634), 241–252.

Halswell, P., Wilson, P.A., Taunton, D.J., Austen, S., 2011. Design and performance of inflatable boats: flexibility and environmental considerations.

Harder, D.L., Speck, O., Hurd, C.L., Speck, T., 2004. Reconfiguration as a prerequisite for survival in highly unstable flow-dominated habitats. J. Plant Growth Regul. 23, 98–107.

Hu, F., Kou, Z., Sefene, E.M., Mikolajczyk, T., 2023. An origami flexiball-inspired soft robotic jellyfish. J. Mar. Sci. Eng. 11 (4), http://dx.doi.org/10.3390/jmse11040714, URL https://www.mdpi.com/2077-1312/11/4/714.

Kim, D.J., Kim, S.Y., You, Y.J., Rhee, K.P., Kim, S.H., Kim, Y.G., 2013. Design of high-speed planing hulls for the improvement of resistance and seakeeping performance. Int. J. Nav. Archit. Ocean Eng. 5 (1), 161–177. http://dx.doi.org/10.2478/IJNAOE-2013-0124.

Korobkin, A.A., Khabakhpasheva, T.I., Maki, K.J., 2017. Hydrodynamic forces in water exit problems. J. Fluids Struct. 69, 16–33.

Kuribayashi, K., Tsuchiya, K., You, Z., Tomus, D., Umemoto, M., Ito, T., Sasaki, M., 2006. Self-deployable origami stent grafts as a biomedical application of Ni-rich TiNi shape memory alloy foil. Mater. Sci. Eng. A 419 (1–2), 131–137.

Ma, X., An, N., Cong, Q., Bai, J.-B., Wu, M., Xu, Y., Zhou, J., Zhang, D., Zhang, T., Guo, R., et al., 2024. Design, modeling, and manufacturing of high strain composites for space deployable structures. Commun. Eng. 3 (1), 78.

Meloni, M., Cai, J., Zhang, Q., Sang-Hoon Lee, D., Li, M., Ma, R., Parashkevov, T.E., Feng, J., 2021. Engineering origami: A comprehensive review of recent applications, design methods, and tools. Adv. Sci. 8 (13), 2000636. http://dx.doi.org/10.1002/advs.202000636.

Miura, K., 2008. Science of Miura-ori: A review. In: Proceedings of 4th International Conference on Origami in Science, Mathematics, and Education. 4OSME.

Paoli, A., Razionale, A.V., 2012. Large yacht hull measurement by integrating optical scanning with mechanical tracking-based methodologies. Robot. Comput.-Integr. Manuf. 28 (5), 592–601. http://dx.doi.org/10.1016/j.rcim.2012.02.010.

Russell, B.R., Thrall, A.P., Padula, J.A., Fowler, J.E., 2014. Reconceptualization and optimization of a rapidly deployable floating causeway. J. Bridge Eng. 19 (4), 04013013.

Savitsky, D., 1985. Planing craft. Nav. Eng. J. 97 (2), 113–141.

Savitsky, D., DeLorme, M.F., Datla, R., 2007. Inclusion of whisker spray drag in performance prediction method for high-speed planing hulls. Mar. Technol. SNAME News 44 (01), 35–56.

Sun, H., Faltinsen, O.M., 2007. The influence of gravity on the performance of planing vessels in calm water. J. Engrg. Math. 58, 91–107.

Tavakoli, S., Zhang, M., Kondratenko, A.A., Hirdaris, S., 2024. A review on the hydrodynamics of planing hulls. Ocean Eng. 303, 117046.

Woodruff, S.R., Filipov, E.T., 2020. A bar and hinge model formulation for structural analysis of curved-crease origami. Int. J. Solids Struct. 204–205, 114–127. http://dx.doi.org/10.1016/j.ijsolstr.2020.08.010.

Woodruff, S.R., Filipov, E.T., 2021. Curved creases redistribute global bending stiffness in corrugations: theory and experimentation. Meccanica 56 (6), 1613–1634.

Zarnick, E.E., 1978. A Nonlinear Mathematical Model of Motions of a Planing Boat in Regular Waves. Technical Report DTNSRDC–78/032, David W. Taylor Naval Ship Research and Development Center, Bethesda, Maryland, URL https://apps.dtic.mil/sti/citations/ADA052039.

Zarnick, E.E., 1979. A Nonlinear Mathematical Model of Motions of a Planing Boat in Irregular Waves. Technical Report DTNSRDC/SPD–0867–01, David W. Taylor Naval Ship Research and Development Center, Bethesda, Maryland, URL https://apps.dtic.mil/sti/citations/ADA078605.

Zirbel, S.A., Trease, B.P., Thomson, M.W., Lang, R.J., Magleby, S.P., Howell, L.H., 2015. Hanaflex: a large solar array for space applications. In: Micro- and Nanotechnology Sensors, Systems, and Applications VII, vol. 9467, SPIE, pp. 179–187.